Analyst

ROYAL SOCIETY OF CHEMISTRY

PAPER

Cite this: *Analyst*, 2020, **145**, 6254

Fluorescent and colorimetric determination of glutathione based on the inner filter effect between silica nanoparticle–gold nanocluster nanocomposites and oxidized 3,3′,5,5′-tetramethylbenzidine†

Guoyan Zhang, Meihao Xiang, Rong-Mei Kong * and Fengli Qu *

Determination of glutathione (GSH) is closely related to the clinical diagnosis of many diseases. Thus, a fluorescent and colorimetric dual-readout strategy for the sensitive determination of glutathione was proposed. The mesoporous silica nanoparticle–gold nanocluster (MSN–AuNC) nanocomposites with significantly enhanced emission and effectively improved photostability characteristics were used as fluorescent probes. Based on the inner filter effect (IFE), the fluorescence of MSN–AuNCs at 570 nm can be effectively quenched by oxidized 3,3′,5,5′-tetramethylbenzidine (oxTMB) with absorption in the wavelength ranges of 330–470 nm and 500–750 nm. However, the addition of GSH could cause the reduction of blue oxTMB to colorless TMB, resulting in the inhibition of IFE and the recovery of the fluorescence of MSN–AuNCs. Therefore, using oxTMB as both quencher and color indicator, a dual-readout oxTMB/MSN–AuNC sensing system for the sensitive determination of GSH was constructed. As signal amplification is caused by the fluorescence enhancement of MSN–AuNCs, the detection limits as low as 0.12 μM and 0.34 μM can be obtained for fluorescent and colorimetric assay, respectively. This method may not only offer a new idea for the sensitive and effective determination of GSH, but also broaden the applications of AuNCs in fluorescent and colorimetric dual-readout bioanalysis.

Received 12th July 2020,
Accepted 3rd August 2020

DOI: 10.1039/d0an01392g

rsc.li/analyst

1. Introduction

Glutathione (GSH) serves many cellular functions, including maintenance of intracellular redox and amino acid homeostasis and conjugation substrate for a variety of endogenous and exogenous substrates. Aberrant levels of GSH can lead to human diseases, such as cancer, heart disease, stroke, and many neurological disorders.[1] Therefore, a series of methods were established for GSH determination, including fluorescence, high performance liquid chromatography (HPLC), mass spectrometry and electrochemistry.[2–7] Although most of these approaches exhibit high sensitivity, they still suffer from some nonnegligible intrinsic shortcomings such as utilization of sophisticated instruments and tedious sample preparation. Hence, many efforts have been made focusing on the development of new fluorescent probes for effective detection of GSH, such as carbon quantum dots (CQDs) that serve as fluorescent signal probes for the determination of GSH because of their good biocompatibility.[8–14] Nevertheless, most of these methods were based on fluorescence "turn-off" mode, resulting in large fluorescence background that limits their practical applications.[15,16] Organic fluorophores can have selectivity for the determination of GSH, but they still have some disadvantages when considering their practical applications in biological samples, for example, use of organic solvent or surfactant and long response time.[17] Therefore, facile and effective measurement methods for fluorescence "turn-on" determination of GSH are still highly desired.

As a new type of fluorescent nanomaterial, metal nanoclusters (NCs) have attracted much attention from researchers owing to their excellent optical properties, good photostability and biocompatibility, large Stokes shifts and facile preparation methods. Therefore, metal NCs are becoming the preferred material for the construction of fluorescence sensors.[18,19] As the fluorescence properties of metal NCs are highly sensitive to their size and environment,[20–22] many methods have been developed to improve the fluorescence intensity and stability of metal NCs. For example, our group has reported an electro-

Key Laboratory of Life-Organic Analysis of Shandong Province, Qufu Normal University, Qufu 273165, China. E-mail: kongrongmei@126.com, fengliquhn@hotmail.com

†Electronic supplementary information (ESI) available. See DOI: 10.1039/d0an01392g

static adsorption based self-assembly of mesoporous silica nanoparticle–gold nanocluster (MSN–AuNC) nanocomposites, which were successfully used for the sensitive determination of heparin.[23] The encapsulated reagents in the mesopore of silica nanoparticles can be protected from the degradative and fluorescence quenching effects of the biological environment,[24,25] making the nanocomposite to exhibit significantly enhanced fluorescence and improved photostability characteristics. Therefore, employing the MSN–AuNC nanocomposite as the fluorescent probe to magnify the fluorescent signal for the determination of GSH could be a very feasible and effective plan.

The fluorescence inner filter effect (IFE) is a well-known phenomenon in which the overlapping of the fluorescence excitation or emission spectra of luminescent species with the absorption spectrum of absorbent species results in fluorescence quenching.[26] Particularly, the fluorescence approach based on the IFE does not require the link of the absorber with the fluorophore, which offers flexibility and facility to construct a biosensor.[27] In addition, the fluorescent and colorimetric dual-readout assay has been widely used in biosensing due to its advantages of high sensitivity and specificity, convenience, and naked eye detection ability.[28,29] Therefore, it is very attractive to develop a simple and sensitive dual-readout method for GSH determination based on the IFE.

Herein, we describe a fluorescent and colorimetric dual-readout assay based on the IFE between oxidized 3,3′,5,5′-tetramethylbenzidine (oxTMB) and MSN–AuNCs for the sensitive quantification of GSH. As shown in Scheme 1, first the self-assembly of a MSN–AuNC nanocomposite was performed *via* the electrostatic interaction between the positively charged amino functionalized MSN and the negatively charged AuNC-stabilizing surface ligand GSH, and the nanocomposite exhibits significantly enhanced fluorescence emission and improved stability. As the absorption spectrum of oxTMB overlaps well with the excitation and emission spectra of MSN–AuNCs, the IFE induced fluorescence quenching of MSN–AuNCs can occur efficiently. However, the introduction of GSH can lead to a concentration-dependent reduction of blue oxTMB ito colorless TMB with a proportional decrease in absorbance. As a result, the efficient fluorescence recovery of the quenched MSN–AuNCs can be observed due to the inhibition of IFE between TMB and MSN–AuNCs. Taking advantage of the fluorescence enhancement of MSN–AuNCs and the effective IFE between oxTMB and MSN–AuNCs, sensitive determination of GSH can be realized. It is worth mentioning that a higher fluorescence of MSN–AuNCs can be observed by the introduction of GSH, which also makes an important contribution to the sensitive determination of GSH. The possible mechanisms have been attributed to the formation of smaller but highly fluorescent Au species that were etched by thiols.[30] In addition, the fluorescent and colorimetric dual-readout method can improve the accuracy and reliability based on the self-confirmation of results.[31,32] Therefore, the integration of these merits in this sensing platform makes the proposed method to act as an outstanding tool for the analysis of GSH.

2. Results and discussion

2.1. Characterization of synthesized nanomaterials

The elementary composition and morphology of synthesized AuNCs and MSN–AuNCs were first characterized by TEM and EDS (Fig. 1). As demonstrated in Fig. 1A, the AuNCs present good spherical monodispersion with an average diameter of about 2 nm. Fig. 1B shows that the amino-functionalized MSNs exhibit nearly uniform spherical morphology with an average size of about 81 nm and a large quantity of mesopores can be obviously observed. Fig. 1C shows that the perfect morphology of MSN–AuNCs still maintained a spherical structure after electrostatic adsorption of AuNCs onto the surface and into the pores of MSNs, confirming that the formation of MSN–AuNC nanocomposites had no effect on the structure of the MSNs. To further confirm the successful loading of AuNCs onto the surface and into the pores of MSNs, nitrogen adsorp-

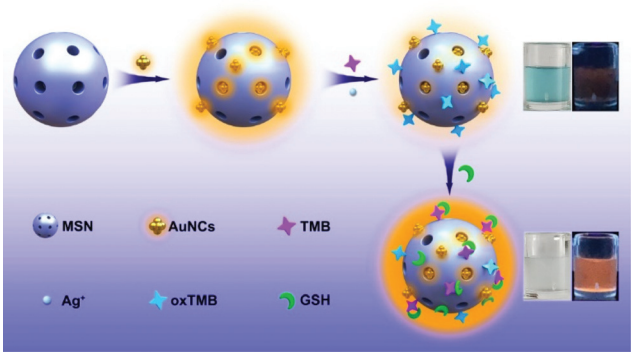

Scheme 1 Schematic illustration of the oxTMB/MSN–AuNC sensing system for fluorescent and colorimetric determination of GSH.

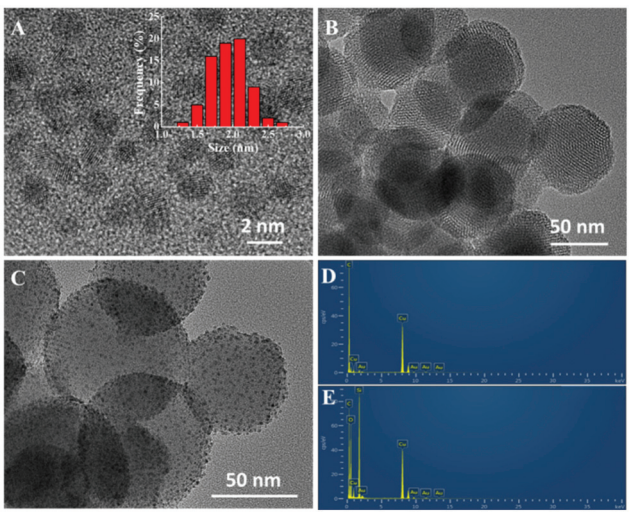

Fig. 1 TEM images of (A) AuNCs, (B) MSNs, (C) MSN–AuNCs. EDS of (D) AuNCs and (E) MSN–AuNCs.

tion–desorption characterization indicates that MSNs possess a mesoporous structure with a surface area of 696.9 m^2 g^{-1}, which decreased to 436.4 m^2 g^{-1} after loading of AuNCs (Fig. S1A†). The average pore size of MSNs was found to be 2.78 nm, whereas no distinguishable pore structure could be identified for MSN–AuNCs (Fig. S1B†), clearly demonstrating the successful loading of AuNCs onto the surface and into the nanopores of MSNs. The EDS energy spectrum was recorded to perform the elemental analysis. The signal of the Au element comes from AuNCs (Fig. 1D), and the distribution of signals from Si, O and Au elements demonstrated that AuNCs were successfully bound by MSN to form the MSN–AuNC nanocomposite (Fig. 1E). The fluorescence spectra were recorded to investigate the fluorescence properties of AuNCs and MSN–AuNC nanocomposites (Fig. 2A). The weak fluorescence emission peak of AuNCs was centered at 570 nm. As expected, the MSN–AuNC nanocomposite exhibits a significantly enhanced fluorescence emission at 570 nm which may be due to the fact that the self-assembly of MSN–AuNC nanocomposites results in the restriction of motion of AuNCs, and the excitation peaks of both of them are located at 365 nm.[33] The inset image of Fig. 2A shows an orange-red emission of MSN–AuNCs which is obviously brighter than that of AuNCs, and is consistent with the fluorescence spectra. The stability of MSN–AuNCs was investigated by placing the nanocomposites for 7 days in the water solution, since the sensor system was constructed in water. The fluorescence intensity at 570 nm was recorded every day at an excitation wavelength of 365 nm. As can be seen from Fig. S2,† the fluorescence intensity almost remained stable and only weakened slightly after 4 days, indicating the photostability characteristics of MSN–AuNCs. In addition, the effect of pH on the fluorescence of MSN–AuNCs was investigated by varying the determination pH at a fixed MSN–AuNC concentration of 0.4 mg mL^{-1} in Tris-HCl buffer (10 mM). As shown in Fig. S3,† the fluorescence intensity of MSN–AuNCs was relatively stable in the pH range of 6.0–8.0 and very similar to that in water. Under the condition of more partial acid or base, the fluorescence intensity slightly decreased to a certain extent, indicating that the MSN–AuNC nanocomposite has stable optical properties in near neutral aqueous solution environments.

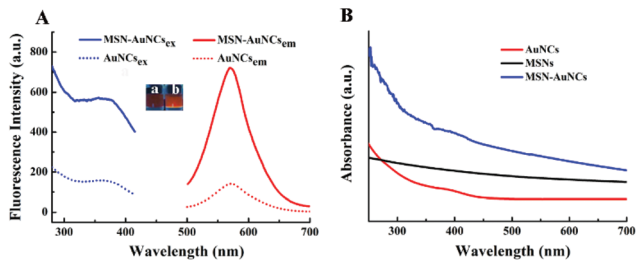

Fig. 2 (A) Fluorescence excitation and emission spectra of AuNCs and MSN–AuNCs. Inset: the fluorescence emission photographs of (a) AuNCs and (b) MSN–AuNCs. (B) UV-Vis absorbance spectra of AuNCs, MSNs and MSN–AuNCs.

In addition, UV–vis absorption spectra were recorded to characterize the synthesis of MSN–AuNC nanocomposites. Fig. 2B shows that the absorption peak of free AuNCs was centered at approximately 375 nm, while MSNs had no absorption peak in the wavelength range of 300–710 nm. Thus, the absorption peak at 375 nm in MSN–AuNCs was attributed to the electrostatic adsorption of AuNCs into the pores and onto the surfaces of MSNs.[23]

2.2. Principle of the sensing system

A novel fluorescent and colorimetric dual-readout assay for the determination of GSH was designed, which may be based on the IFE between MSN–AuNCs and oxTMB (Scheme 1). The spectral information was investigated first to confirm the IFE principle for GSH determination. As shown in Fig. 3, the fluorescence excitation spectrum centered at 365 nm and the emission spectrum centered at 570 nm of MSN–AuNCs overlap well with the absorption spectrum of oxTMB in the wavelength ranges of 330–470 nm and 500–750 nm, indicating the IFE occurrence possibility between MSN–AuNCs and oxTMB. However, TMB only shows an absorption peak at about 285 nm, which perfectly avoids overlap with the fluorescence excitation and emission spectrum of MSN–AuNCs. Therefore, the IFE can be inhibited between MSN–AuNCs and TMB. During the process of IFE, it is well known that almost no fluorescence lifetime decline of the fluorophore can be observed.[34] Therefore, the fluorescence lifetime of MSN–AuNCs was measured in the absence and presence of oxTMB. As shown in Fig. S4A,† there is no fluorescence lifetime change of MSN–AuNCs in the presence of oxTMB, which was reasonable to support the IFE-based contribution to the fluorescence quenching of MSN–AuNCs.[35] To further confirm the IFE quenching mechanism, the surface charges of MSN–AuNCs and oxTMB were characterized *via* zeta potential measurements.[34,36] As shown in Fig. S4B,† the zeta potentials of GSH-capped AuNCs and amino-functionalized MSNs are −17.9 mV and +30.3 mV, respectively. The MSN–AuNC nanocomposite that was obtained by simple mixing of AuNCs and

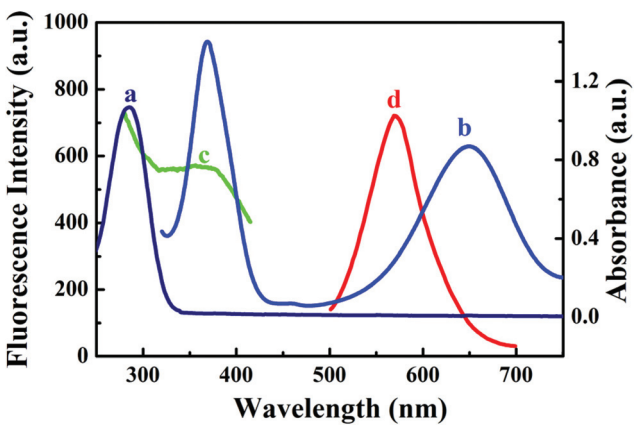

Fig. 3 UV-Vis absorbance spectra of (a) TMB and (b) oxTMB; fluorescence (c) excitation and (d) emission spectra of MSN–AuNCs.

MSNs exhibits a small positive zeta potential of about +4.6 mV, indicating the good electrostatic adsorption between them. As expected, oxTMB is also positively charged with a zeta potential of +11.2 mV, which indicates the electrostatic repulsion between MSN–AuNCs and oxTMB. Therefore, the zeta potential measurement results further prove the IFE caused fluorescence quenching of MSN–AuNCs by oxTMB.

2.3. The feasibility of the sensing system

The feasibility of the sensing system for fluorescent and colorimetric dual-readout determination of GSH was confirmed by fluorescence spectrum (Fig. 4A) and UV-Vis absorption spectrum (Fig. 4B) investigation. Fig. 4A manifests that the fluorescence intensity of MSN–AuNCs (curve b) was almost 5 times larger than AuNCs (curve a). When a certain concentration of oxTMB (800 μM) was added to the MSN–AuNC solution, the fluorescence of MSN–AuNCs was strongly quenched (curve c). However, the introduction of GSH (100 μM) into the oxTMB/MSN–AuNC system resulted in the recovery of fluorescence of MSN–AuNCs due to the reduction of oxTMB to TMB by GSH and the inhibition of IFE (curve d). Even more noteworthy is the fact that when a high concentration of GSH (1 mM) was added to the oxTMB/MSN–AuNC solution, the fluorescence of MSN–AuNCs was recovered even larger than that of MSN–AuNCs (curve e). The inset of Fig. 4A shows the corresponding fluorescence photographs (under 365 nm light) of the above solutions, which were consistent with the fluorescence measurements. According to previous reports,[30,37] the presence of GSH could lead to the etching of AuNCs thus resulting in fluorescence enhancement and red-shift. Therefore, TEM images and fluorescence emission spectra were recorded for AuNCs and MSN–AuNCs before and after etching by GSH to characterize the nanomaterial size and fluorescence changes. As shown in Fig. S5,† the size of AuNCs decreased from about 2 nm to 1 nm after the addition of 1 mM GSH, and the AuNCs adsorbed by MSN to form MSN–AuNCs were also etched by GSH and they became smaller (Fig. S6†). The corresponding fluorescence of AuNCs and MSN–AuNCs were obviously enhanced after the addition of GSH and were red-shifted from 570 to about 573 and 572 nm, respectively (Fig. S5C and S6C†). The results further indicate the etching effect of GSH on AuNCs, which is another important contribution to fluorescence recovery for the determination of GSH. Fig. 4B shows the absorption spectra of the sensing system under different conditions. It can be clearly seen that AuNCs have no obvious absorption peak in the wavelength range of 500–750 nm (curve a) and none of MSN–AuNCs (curve b), and their solutions were all colourless and transparent. After the addition of oxTMB (800 μM) to the MSN–AuNC solution, the absorption peak at 652 nm that is ascribed to oxTMB appeared (curve c), and the colour of the oxTMB/MSN–AuNC solution turned blue. However, the introduction of GSH (100 μM) induced a significant decrease in absorption at 652 nm (curve d), along with the fading of the colour of the mixed solution. Therefore, the results confirmed that the oxTMB/MSN–AuNC sensing system can be used for the fluorescent and colorimetric dual-readout determination of GSH.

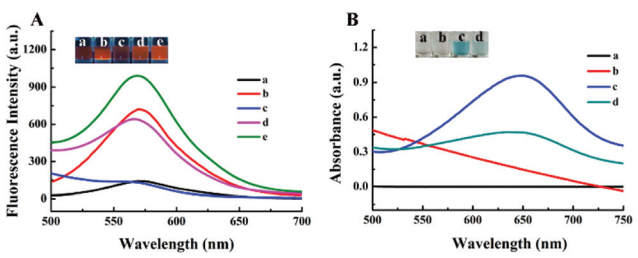

Fig. 4 (A) Fluorescence emission spectra of (a) AuNCs, (b) MSN–AuNCs, (c) MSN–AuNCs + oxTMB (800 μM), (d) MSN–AuNCs + oxTMB (800 μM) + GSH (100 μM) and (e) MSN–AuNCs + oxTMB (800 μM) + GSH (1 mM). The inset photographs correspond to the fluorescence emission spectra. (B) UV-vis absorbance spectra of (a) AuNCs, (b) MSN–AuNCs, (c) MSN–AuNCs + oxTMB (800 μM) and (d) MSN–AuNCs + oxTMB (800 μM) + GSH (100 μM). The inset photographs correspond to the UV-vis absorbance spectra.

2.4. Optimization of assay conditions

In order to obtain the best sensing performance for GSH, the determination parameters were optimized including the concentrations of MSNs and oxTMB, the reaction time between MSN–AuNCs and oxTMB and the incubation time for GSH determination (Fig. S7†). Since the fluorescence signal is offered by the AuNCs aggregated in the pores and on the surfaces of MSNs, the MSN concentration was first optimized by fixing the volume of AuNCs (0.84 mg mL^{-1}) at 50 μL while varying the MSN concentration from 0.1 mg mL^{-1} to 0.6 mg mL^{-1} to get the best assay conditions. As shown in Fig. S7A,† with an increase in the MSN concentration, the fluorescence intensity at 570 nm gradually increased, and when the MSN concentration was 0.4 mg mL^{-1}, the fluorescence reached the maximum value and no longer increased with the increase in the concentration of MSNs, indicating the saturated loading of AuNCs by MSNs. Therefore, 0.4 mg mL^{-1} MSN was used in the following experiments. Fig. S7B† shows the relationship between the fluorescence quenching and the reaction time of adding oxTMB to MSN–AuNCs. The stable fluorescence quenching could be obtained after 5 min, indicating that the reaction between oxTMB and MSN–AuNCs is stable. Next, the quenching efficiency of oxTMB for MSN–AuNCs was investigated by varying the oxTMB concentration in the range of 50 μM to 1 mM, and from the result shown in Fig. S7C† it can be seen that 800 μM of oxTMB could result in the quenching of the fluorescence intensity of MSN–AuNCs to the minimum. Finally, the incubation time for GSH determination was optimized, and the result indicated that the fluorescence intensity was restored to the maximum value and remained stable when the incubation time was 10 min (Fig. S7D†). Therefore, 10 min was chosen as the optimal incubation time for the determination of GSH using this sensing system.

2.5. Performance for GSH determination

The performance of the current strategy for the quantitative determination of GSH was investigated under optimized con-

ditions. To ensure the reliability of the experiment, 3 parallel tests were performed for each determination. As illustrated in Fig. 5A, the fluorescence signal of MSN–AuNCs was gradually recovered when the GSH concentration increased in the range from 1 μM to 1 mM. Interestingly, when the concentration of GSH exceeds 100 μM, the restored fluorescence intensity will exceed the fluorescence intensity of the MSN–AuNC nanocomposite itself, maybe, which attributed to the fluorescence enhancement induced by GSH induced etching of AuNCs.[30] Meanwhile, with the increase of GSH concentration, the emission wavelength of the system undergoes a small degree of red-shift, which is consistent with the reference report.[37] The inset shows that the photographs of fluorescent color change under 365 nm light for the determination of GSH with different concentrations were consistent with the results for fluorescence spectra. Meanwhile, visual readout for the fluorescent color change under 365 nm light can be achieved. As shown in Fig. 5B, good linear relationships between the fluorescence intensity at 570 nm and the concentration of GSH in two ranges of 1 μM–50 μM and 50 μM–1 mM can be found, respectively. The corresponding regression equations are F = 197.2 + 161.1 $\mathrm{LgC_{GSH}}$ (μM) with an R^2 value of 0.989 and F = −251.9 + 436.2 $\mathrm{LgC_{GSH}}$ (μM) with an R^2 value of 0.985. The detection limit of GSH was estimated to be 0.12 μM using the low concentration calibration range according to the 3σ rule. The two linear ranges for GSH with two different slopes may be due to the difference in the reaction rates between the two concentration ranges. In the low concentration range of GSH, a small amount of oxTMB can be reduced, so that the fluorescence of MSN–AuNCs is almost quenched by oxTMB, thus presenting a slower fluorescence recovery rate, whereas, when the concentration of GSH is gradually increased, most of oxTMB can be reduced to TMB, resulting in the inhibition of IFE between MSN–AuNCs and oxTMB, so that the fluorescence of MSN–AuNCs is rapidly recovered.

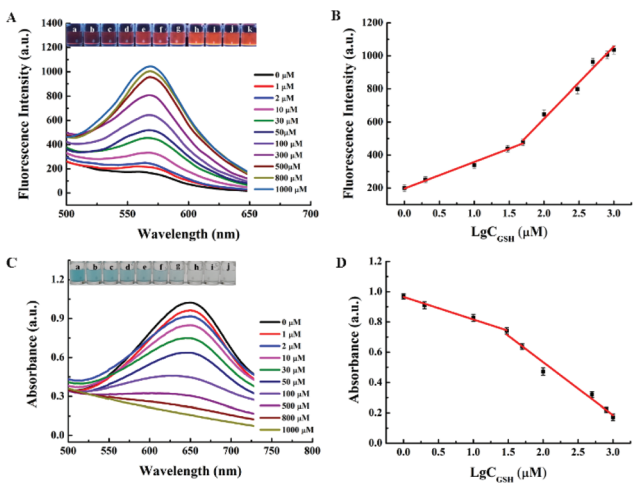

Fig. 5 The fluorescent spectra (A) and UV-vis absorbance spectra (C) of the sensing system in the presence of different concentrations of GSH. (B) Linear relationship between GSH concentration and fluorescence intensity at 570 nm. Inset: the concentrations of GSH in fluorescence photographs from a to k are 0, 1, 2, 10, 30, 50, 100, 300, 500, 800 and 1000 μM, respectively. (D) Linear relationship between GSH concentration and absorbance intensity at 652 nm. Inset: the concentrations of GSH in fluorescence photographs from a to j are 0, 1, 2, 10, 30, 50, 100, 500, 800 and 1000 μM, respectively. The error bars were estimated from three replicate measurements.

The UV-Vis spectra of each reaction solution with different concentrations of GSH are shown in Fig. 5C. In the absence of GSH, the oxTMB/MSN–AuNC solution presented a strong absorption peak at 652 nm in the wavelength range of 500–700 nm. However, with an increase in the concentration of GSH, the absorption peak at 652 nm gradually disappeared due to the reduction of oxTMB to TMB. As shown in Fig. 5D, a 2-stage linear relationship between the absorption intensity at 652 nm and the GSH concentration was obtained due to the different reaction speeds caused by the same reasons as the fluorescence determination. The corresponding regression equations are A = 0.966–0.1494 $\mathrm{LgC_{GSH}}$ (μM) with an R^2 value of 0.990 in the range of 1 μM–30 μM and A = 1.233–0.349 $\mathrm{LgC_{GSH}}$ (μM) with an R^2 value of 0.980 in the range of 30 μM–1 mM. The detection limit is estimated to be 0.34 μM using the low concentration calibration range, at the same time, the color of the solution gradually turns from initial blue to colorless (Fig. 5C, inset), and the color change caused by approximately 30 μM GSH can be easily distinguished by the naked eye. When compared with several reported fluorescent and colorimetric methods for GSH determination (Table S1†), this nanosensor not only showed sufficient sensitivity for GSH but also avoided tedious operations due to the effective photostability of MSN–AuNCs as well as its unique property of electrostatic interaction. More importantly, as the determination results can also be observed with the naked eye in the dual signal sensing system, it is beneficial for semiquantitative measurement when the detecting instrument is limited. These advantages make this sensor a candidate for GSH determination.

To study the selectivity of oxTMB/MSN–AuNC sensing system for GSH determination, several amino acids and some possible coexisting substances were used to investigate the effects. As shown in Fig. 6, compared with the significant fluorescence enhancement of the oxTMB/MSN–AuNC sensing system induced by GSH, the presence of interfering substances caused only small fluorescence changes except 50 μM AA which caused a certain extent of fluorescence enhancement. Fortunately, when the concentration of AA was reduced to 20 μM and 10 μM, its influences were all decreased obviously. Moreover, the concentration of AA in human serum is much lower than that of GSH.[38–42] Therefore, in the diluted human serum, the concentration of AA is not sufficient to cause significant interference for GSH determination. Therefore, the application of this probe in human serum samples has great potential.

2.6. Determination of GSH in human serum samples

To investigate the application of the oxTMB/MSN–AuNC sensing system in the biological environment, the human

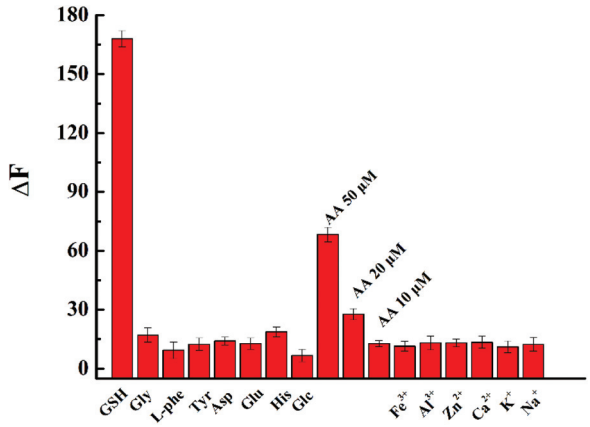

Fig. 6 Selectivity investigation of the sensing system for the determination of GSH. The concentration of GSH is 10 μM, that of amino acids and AA are all 50 μM, and that of metal ions are all 500 μM. The error bars were estimated from three replicate measurements.

Table 1 Determination of GSH in human serum samples

Sample	Added (μM)	Measure (μM)	Recovery (%)	RSD (%, n = 3)
1	1	0.97	97.0	3.3
2	5	4.93	98.6	2.8
3	10	10.52	105.2	3.2
4	50	50.34	100.6	4.1
5	100	103.65	103.7	2.5

serum was collected by centrifugation at 15 000 rpm for 10 min. The sample was prediluted to be consistent with the range of our assay, which can not only reduce the required sample amount but also decrease the interference of the complex matrix in serum. Under optimal experimental conditions, 1 μM, 5 μM, 10 μM, 50 μM, and 100 μM of GSH were spiked into the diluted serum samples, respectively, and then added to the oxTMB/MSN–AuNC sensing system. The experimental procedure was the same as that in water solution. The determination results are shown in Table 1. The recoveries after the addition of different concentrations of GSH to human serum samples were between 97% and 105.2% and the relative standard deviation (RSD) values were all lower than 4.1%, which demonstrated the application potential of the oxTMB/MSN–AuNC sensing system in human serum.

3. Conclusions

A target has been constructed to develop a flexible and sensitive approach for the determination of GSH. So, we have demonstrated a novel fluorescent and colorimetric dual-readout oxTMB/MSN–AuNC sensing system which can achieve more sensitive and intuitionistic determination of GSH. The experimental results showed a good linear relationship between the fluorescence absorbance and the GSH concentration, and also demonstrated the promising potential application of this system in real biological systems. Based on the IFE strategy, the proposed method can be expanded to detect various targets by using MSN–AuNCs.

4. Experimental section

4.1. Materials and Instruments

3,3′,5,5′-Tetramethylbenzidine (TMB), glutathione (GSH) (reduced form) and chloroauric acid ($HAuCl_4$) were purchased from Aladdin Industrial Inc. (Shanghai, China, http://www.aladdin-e.com). Tetraethyl orthosilicate (TEOS), (3-aminopropyl) triethoxysilane (APTES), hexadecyl trimethylammonium bromide (CTAB), glucose (Glc), glycine (Gly), aspartic acid (Asp), tyrosine (Tyr), L-phenylalanine (L-phe), lysine (Lys), histidine (His), glutamic acid (Glu) and ascorbic acid (AA) were purchased from Sigma-Aldrich (St Louis Missouri, USA, https://www.sigmaaldrich.com). Methanol, sodium hydroxide (NaOH), silver nitrate ($AgNO_3$), sodium chloride (NaCl), potassium chloride (KCl), calcium chloride ($CaCl_2$), zinc chloride ($ZnCl_2$), magnesium chloride ($MgCl_2$), aluminium chloride ($AlCl_3$) and ferric trichloride ($FeCl_3$) were purchased from Sinopharm Chemical Reagent Co. Ltd (Shanghai, China, http://www.sino-reagent.com). The buffer used in this work was 10 mM Tris-HCl, The pH was measured using a Mettler-Toledo Delta 320 pH meter. Other reagents were of analytical grade and used without further purification. All aqueous solutions were prepared with deionized water (resistivity >18 MΩ cm) produced using a Millipore system.

UV–vis spectra were recorded using a Varian cary-300 UV-vis spectrophotometer. Morphological characterization of the as-prepared materials were performed using a transmission electron microscope (TEM, JEM-2100PLUS, Japan). All fluorescence measurements were carried out using an F-7000 spectrometer (Hitachi, Japan) operated at an excitation wavelength of 365 nm, with both excitation and emission slit widths of 5.0 nm and at a PMT detector voltage of 700 V. The fluorescence photos were obtained using a ZF-1B box-like ultraviolet analyzer (Shanghai, China).

4.2. Synthesis of AuNCs and amino-functionalized MSNs

AuNCs were synthesized according to the method reported by the Xie group with slight modification.[37] The amino-functionalized MSNs were synthesized by co-condensation in alkaline solution.[43] For synthesis details see ESI.†

4.3. Fluorescence determination of GSH

Fluorescence determination of GSH was performed as follows: Typically, 450 μL of ultrapure water, 200 μL of MSN solution (2 mg mL^{-1}) and 50 μL of AuNC solution (0.84 mg mL^{-1}) were mixed in a 2 mL centrifuge tube and gently shaken in a thermostatic oscillator at 25 °C for 30 min. Meanwhile, oxTMB (4 mM) was prepared by adding TMB solution to $AgNO_3$ solu-

tion (the molar ratio was 4 : 1) in a 10 mL centrifuge tube. After that, 200 μL of oxTMB was added to the above-prepared MSN–AuNC solution and gently shaken in a thermostatic oscillator at 25 °C for 10 min. Next, 100 μL of GSH solutions at different concentrations were added to the as-mentioned solution and gently shaken for 10 min at 25 °C. Finally, the fluorescence spectra were recorded at an excitation wavelength of 365 nm and emission wavelength of 570 nm. The practicality investigation of the fluorescence method for GSH detection was conducted in human serum samples which was provided by the Qufu Normal University School Hospital. Serum experiments were performed according to the Guidelines for Ethical Committee of Qufu Normal University. All studies were approved by the Ethical Committee of Qufu Normal University. Informed consent was obtained from the human participants of this study.

Conflicts of interest

The author(s) declare that they have no competing interests.

Acknowledgements

This work was supported by the National Natural Science Foundation of China (21775089) and the Natural Science Foundation of Shandong Province (ZR2017JL010 and ZR2017QB008) and Taishan Scholar of Shandong Province (tsqn201909106).

Notes and references

1 Z. Zhang, Y. Jiao, Y. Wang and S. Zhang, *Sci. Rep.*, 2016, **6**, 29872.
2 Y. V. Tcherkas, A. D. Denisenko and J. Chromatogr, *A*, 2001, **913**, 309–313.
3 N. Burford, M. D. Eelman, D. E. Mahony and M. Morash, *Chem. Commun.*, 2003, 146–147.
4 W. Zhu, G. Jiang, L. Xu, B. Li, Q. Cai, H. Jiang and X. Zhou, *Anal. Chim. Acta*, 2015, **886**, 37–47.
5 N. K. Wawegama, G. F. Browning, A. Kanci, M. S. Marenda and P. F. Markham, *Clin. Vaccine Immunol.*, 2014, **21**, 196–202.
6 S. Qi, W. Liu, P. Zhang, J. Wu, H. Zhang, H. Ren and P. Wang, *Sens. Actuators, B*, 2018, **270**, 459–465.
7 Q. Tan, R. Zhang, R. Kong, W. Kong, W. Zhao and F. Qu, *Microchim. Acta*, 2018, **185**, 44.
8 Y. Liu, W. Liu, W. Song, J. Liu, C. Ren, J. Wu, D. Liu and H. Liu, *ACS Appl. Mater. Interfaces*, 2017, **9**, 12663–12672.
9 G. Li, H. Fu, X. Chen, P. Gong, G. Chen, L. Xia and Y. Wu, *Anal. Chem.*, 2016, **88**, 2720–2726.
10 Z. Qian, L. Chai, Y. Huang, C. Tang, J. Shen, J. Chen and H. Feng, *Biosens. Bioelectron.*, 2015, **68**, 675–680.
11 Y. Hu, X. Geng, L. Zhang, Z. Huang, J. Ge and Z. Li, *Sci. Rep.*, 2017, **7**, 5849.
12 X. Chen, S. Yu, L. Yang, J. Wang and C. Jiang, *Nanoscale*, 2016, **8**, 13669–13677.
13 Y. Wang, C. Zhang, X. Chen, B. Yang, L. Yang, C. Jiang and Z. Zhang, *Nanoscale*, 2016, **8**, 5977–5984.
14 Y. Wang, Y. Zhu, S. Yu and C. Jiang, *RSC Adv.*, 2017, **7**, 40973–40989.
15 F. Niu, Y. Ying, X. Hua, Y. Niu, Y. Xu and Y. Long, *Carbon*, 2018, **127**, 340–348.
16 Z. Amouzegar, A. Afkhami and T. Madrakian, *Microchim. Acta*, 2019, **186**, 205.
17 F. Wang, L. Zhou, C. Zhao, R. Wang, Q. Fei, S. Luo, Z. Guo, H. Tian and W. Zhu, *Chem. Sci.*, 2015, **6**, 2584–2589.
18 Y. Hu, X. Geng, L. Zhang, Z. Huang, J. Ge and Z. Li, *Sci. Rep.*, 2017, **7**, 5849.
19 P. Karfa, E. Roy, S. Patra, D. Kumar, R. Madhuri and P. K. Sharma, *Biosens. Bioelectron.*, 2016, **78**, 454–463.
20 L. Shang, S. Dong and G. U. Nienhaus, *Nano Today*, 2011, **6**, 401–418.
21 E. Saouter and B. Blattmann, *Anal. Chem.*, 1994, **66**, 2031–2037.
22 J. Yang, T. Yang, X. Wang, M. Chen, Y. Yu and J. Wang, *Anal. Chem.*, 2018, **99**, 6945–6951.
23 L. Ma, M. Zhang, A. Yang, Q. Wang, F. Qu, F. Qu and R. Kong, *Analyst*, 2018, **143**, 5388–5394.
24 L. Lin, Y. Hu, L. Zhang, Y. Huang and S. Zhao, *Biosens. Bioelectron.*, 2017, **94**, 523–529.
25 X. Wang, J. Xia, C. Wang, L. Liu, S. Zhu, W. Feng and L. Li, *ACS Appl. Mater. Interfaces*, 2017, **9**, 44856–44863.
26 S. Yang, C. Wang, C. Liu, Y. Wang, Y. Xiao, J. Li and R. Yang, *Anal. Chem.*, 2014, **86**, 7931–7938.
27 L. Shang and S. Dong, *Anal. Chem.*, 2009, **81**, 1465–1470.
28 C. Chen, D. Zhao, B. Wang, P. Ni, Y. Jiang, C. Zhang, F. Yang, Y. Lu and J. Sun, *Anal. Chem.*, 2020, **92**, 4639–4646.
29 P. Ni, C. Chen, Y. Jiang, C. Zhang, B. Wang, B. Cao, C. Li and Y. Lu, *Sens. Actuators, B*, 2019, **301**, 127080.
30 H. Jiang, X. Su, Y. Zhang, J. Zhou, D. Fang and X. Wang, *Anal. Chem.*, 2016, **88**, 4766–4477.
31 X. Yan, D. Kong, R. Jin, X. Zhao, H. Li, F. Liu and G. Lu, *Sens. Actuators, B*, 2019, **290**, 640–647.
32 H. Wang, X. Wu, S. Yang, H. Tian, Y. Liu and B. Sun, *Food Chem.*, 2019, **286**, 322–328.
33 X. Han, M. Han, L. Ma, F. Qu, R. Kong and F. Qu, *Talanta*, 2019, **194**, 55–62.
34 M. Wang, S. Wang, L. Li, G. Wang and X. Su, *Talanta*, 2020, **207**, 120315.
35 H. Yang, F. Lu, Y. Sun, Z. Yuan and C. Lu, *Anal. Chem.*, 2018, **90**, 12846–12853.
36 Q. Liu, X. Yan, Q. Lai and X. Su, *Sens. Actuators, B*, 2019, **282**, 45–51.
37 Z. Luo, X. Yuan, Y. Yu, Q. Zhang, D. T. Leong, J. Y. Lee and J. Xie, *J. Am. Chem. Soc.*, 2012, **134**, 16662–16670.
38 W. Kong, D. Wu, G. Li, X. Chen, P. Gong, Z. Sun, G. Chen, L. Xia, J. You and Y. Wu, *Talanta*, 2017, **165**, 677–684.
39 L. Li, Q. Wang and Z. Chen, *Microchim. Acta*, 2019, **186**, 257.

40 Q. Cai, J. Li, J. Ge, L. Zhang, Y. Hu, Z. Li and L. Qu, *Biosens. Bioelectron.*, 2015, **72**, 31–36.
41 C. Peng, H. Xing, X. Fan, Y. Xue, J. Li and E. Wang, *Anal. Chem.*, 2019, **91**, 5762–5767.
42 A. Senft, T. P. Dalton and H. G. Shertzer, *Anal. Biochem.*, 2000, **280**, 80–86.
43 X. Ma, S. Sreejith and Y. Zhao, *ACS Appl. Mater. Interfaces*, 2013, **5**, 12860–12868.